Actuator Management in Tokamaks via Receding-Horizon Optimization

A. Pajares, E. Schuster

Lehigh University, Bethlehem, Pennsylvania, USA

Introduction

Efficient and safe operation of reactor-grade tokamaks such as ITER will require optimal management of the available actuators in order to fulfill the required control objectives. This is a particularly difficult control-design challenge due to the multitude of control tasks that share the device actuators. In addition, the appearance of off-normal events and exceptions (due to changes in the plasma state and/or actuator trips) normally makes off-line scenario planning insufficient and requires real-time optimization solutions for actuator management (AM). Previous work where AM algorithms were developed includes [1, 2, 3, 4].

General Description of the AM Scheme

In this work, an AM algorithm based on a real-time, receding-horizon optimization approach is presented (see Fig. 1). A number N of independently-designed controllers compute high-level control requests, such as the total injected power (denoted by P_{tot}) required by an energy controller, or the Neutral Beam Injection (NBI) torque (denoted by T_{NBI}) required by a rotation controller. Therefore, the goal of the high-level control requests, denoted as R_i ($i = 1, \ldots, N$), is to fullfil the particular control goals of the controllers. The requests R_i are sent to the AM algorithm, where they are embedded into a finite, receding-horizon optimization problem. This is done by equating R_i with its associated virtual-input function, F_i, which in general depends on the plasma state, x, controllable input, u, and time, t. As opposed to the individual controllers, which compute high-level requests (i.e. R_i) that fulfill specific control goals, the main objective of the AM algorithm is much more general, as it tries to find the low-level actuator-requests (i.e. the controllable input u) that fulfill as many of the high-level control requests as possible, also taking into account the actuator availability and control-request priorities. At the same time, physical saturation limits constrain the achievable u. Thus, it can be seen that the AM problem can be naturally posed as an optimization problem. Finally, a performance metric, f, that depends on the difference between the predicted and target states (i.e., it varies with x) as well as on the control effort (i.e., it varies with u) is minimized over the prediction horizon.

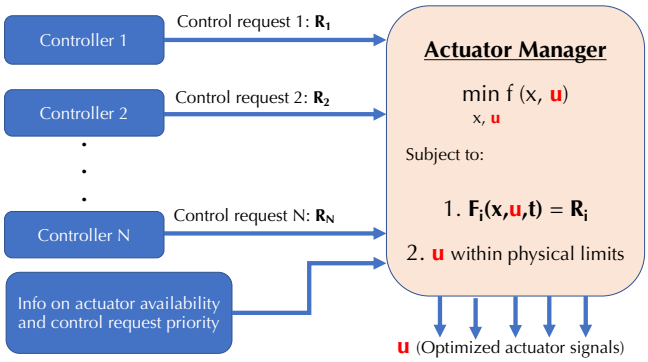

Figure 1: *General architecture with controllers and AM.*

Control Requests: Safety Factor, Bulk Toroidal-Rotation, and Normalized-Beta Control

The AM algorithm proposed in this work can, in principle, be used with any number of controllers and actuators. However, in order to illustrate the AM problem in this paper, it is particularized for the case of combined bulk toroidal-rotation (Ω_ϕ) + normalized beta (β_N) + safety-factor (q) control using three NBI groups. Therefore, three controllers are considered (i.e. $N=3$): (i) Ω_ϕ controller, (ii) β_N controller, and (iii) model-predictive controller (MPC) for q-profile regulation. The controllers' goal is to drive Ω_ϕ, β_N, and q toward their respective targets, $\bar{\Omega}_\phi$, $\bar{\beta}_N$, and $\bar{q}$. For convenience, the poloidal-flux gradient, $\theta \triangleq -B_{\phi,0}\rho_b\rho/q$, is employed instead of q, where $B_{\phi,0}$ is a reference magnetic field and ρ_b is the value of the spatial coordinate ρ at the last closed magnetic-flux surface (see Fig. 2). Also, $\bar{\theta} \triangleq -B_{\phi,0}\rho_b\rho/\bar{q}$ is the θ target derived from $\bar{q}$. The error variables $\tilde{\Omega}_\phi \triangleq \Omega_\phi - \bar{\Omega}_\phi$, $\tilde{\beta}_N \triangleq \beta_N - \bar{\beta}_N$, and $\tilde{\theta} \triangleq \theta - \bar{\theta}$ compose the state vector, i.e. $x = [\tilde{\Omega}_\phi, \tilde{\beta}_N, \tilde{\theta}]$, whereas u contains the feedback (FB) powers of the NBIs, i.e. $u = [P^{FB}_{NBI,1}, P^{FB}_{NBI,2}, P^{FB}_{NBI,3}]$.

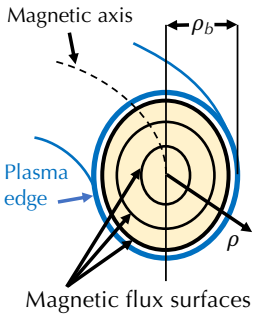

Figure 2: *1D magnetic-flux surface configuration in tokamaks.*

The Ω_ϕ controller computes the FB NBI-torque as $R_1 \triangleq T^{FB}_{NBI} = -K_P^{\Omega_\phi}\tilde{\Omega}_\phi - K_I^{\Omega_\phi}\int_0^t \tilde{\Omega}_\phi dt$, where $K_P^{\Omega_\phi}, K_I^{\Omega_\phi} > 0$ are design parameters. The associated virtual-input function is given by $F_1(u) = k_{NBI,1}P^{FB}_{NBI,1} + k_{NBI,2}P^{FB}_{NBI,2} + k_{NBI,3}P^{FB}_{NBI,3}$, where $k_{NBI,i}$ are constants that model how each NBI injects torque (i.e. $k_{NBI,i} > 0$ for co-I_p and $k_{NBI,i} < 0$ for counter-I_p NBIs). The β_N controller computes the FB total power as $R_2 \triangleq P^{FB}_{tot} = -K_P^{\beta_N}\tilde{\beta}_N - K_I^{\beta_N}\int_0^t \tilde{\beta}_N dt$, where $K_P^{\beta_N}, K_I^{\beta_N} > 0$ are design parameters. Its virtual-input function is $F_2(u) = P^{FB}_{NBI,1} + P^{FB}_{NBI,2} + P^{FB}_{NBI,3}$. Finally, the MPC model is similar to that in [6], where the q-profile dynamics is discretized over m spatial nodes, $[\rho_1, ..., \rho_m]$. The θ dynamics can be written as $F_3(x,u,t) = \frac{d\hat{\theta}}{dt} - G(\hat{\theta},t)u = 0$ (so $R_3 = 0$), where $\hat{\theta} \triangleq [\tilde{\theta}(\rho_1), ..., \tilde{\theta}(\rho_m)]^T$ and $G \in \mathbb{R}^{m\times 3}$ is a model matrix that depends on $\hat{\theta}$ and t [6].

Actuator Management as a Real-Time, Finite-Receding-Horizon Optimization Problem

The state x is sampled at t^k (for $k = 1, 2, 3, ...$), and an optimization problem is solved,

$$\min_{x,u} \int_{t^k}^{t^k+T} \left(x^T Q x + u^T R u\right) dt, \quad \textbf{subject to:} \tag{1}$$

$$F_1(u^k) = k_{NBI,1}P^k_{NBI,1} + k_{NBI,2}P^k_{NBI,2} + k_{NBI,3}P^k_{NBI,3} = -K_P^{\Omega_\phi}\tilde{\Omega}^k_\phi - K_I^{\Omega_\phi}\int_0^{t^k} \tilde{\Omega}_\phi dt \triangleq R_1, \tag{2}$$

$$F_2(u^k) = P^k_{NBI,1} + P^k_{NBI,2} + P^k_{NBI,3} = -K_P^{\beta_N}\tilde{\beta}^k_N - K_I^{\beta_N}\int_0^{t^k} \tilde{\beta}_N dt \triangleq R_2, \tag{3}$$

$$F_3(x^p, u^p, t^p) \approx \frac{\hat{\theta}(t^{p+1}) - \hat{\theta}(t^p)}{\Delta t} - G^p u^p = 0 \triangleq R_3 \quad (\text{for } p = k, k+1, ..., k+M-1), \tag{4}$$

Physical saturation limits: $u \in \mathscr{U}$ (5)

where $T = M\Delta t$ is the horizon (where Δt is the sampling time and $M > 0$ is an integer, so $t^{k+M} \triangleq T$), $Q \in \mathbb{R}^{(2+m)\times(2+m)}$ and $R \in \mathbb{R}^{3\times 3}$ are design matrices that may change in real time according to the actuator-request priorities and actuator availability, $(\cdot)^k$ denotes particularization at t^k, and $\mathscr{U}$ is the feasible set for u. Thus, (1)-(5) provides an estimation for the state, x^p $(k < p \leq k+M)$, together with the control actions, u^p $(k \leq p \leq k+M)$. The value of u at t^k (i.e. u^k) is maintained from t^k till the next sample at t^{k+1}, when u is updated by solving (1)-(5) again.

Simulation Testing using COTSIM

Nonlinear, one-dimensional (1D) simulations have been carried out using the Control-Oriented Transport SIMulator (COTSIM©) for an Advanced Tokamak (AT) scenario in the DIII-D tokamak. The three NBI groups correspond to the on-axis co-I_p NBIs ($P_{NBI,1}$), off-axis co-I_p NBIs ($P_{NBI,2}$), and counter-I_p NBIs ($P_{NBI,3}$) available in DIII-D. First, a feedforward-only (FF-only) simulation is executed with the experimental inputs from DIII-D shot 172538. Second, another FF-only simulation is run with a different set of inputs with lower $P_{NBI,1}$, higher $P_{NBI,2}$, and a step in $P_{NBI,3}$ at $t = 3.5$ s. The evolutions for β_N, Ω_ϕ, and q in this second simulation are set as targets $\bar{\beta}_N$, $\bar{\Omega}_\phi$, and $\bar{q}$ for a third simulation in FF + FB, which is executed to try to drive x toward $\bar{x}$ using the FF inputs of the first simulation. The FB controllers come on at $t = 0.7$ s.

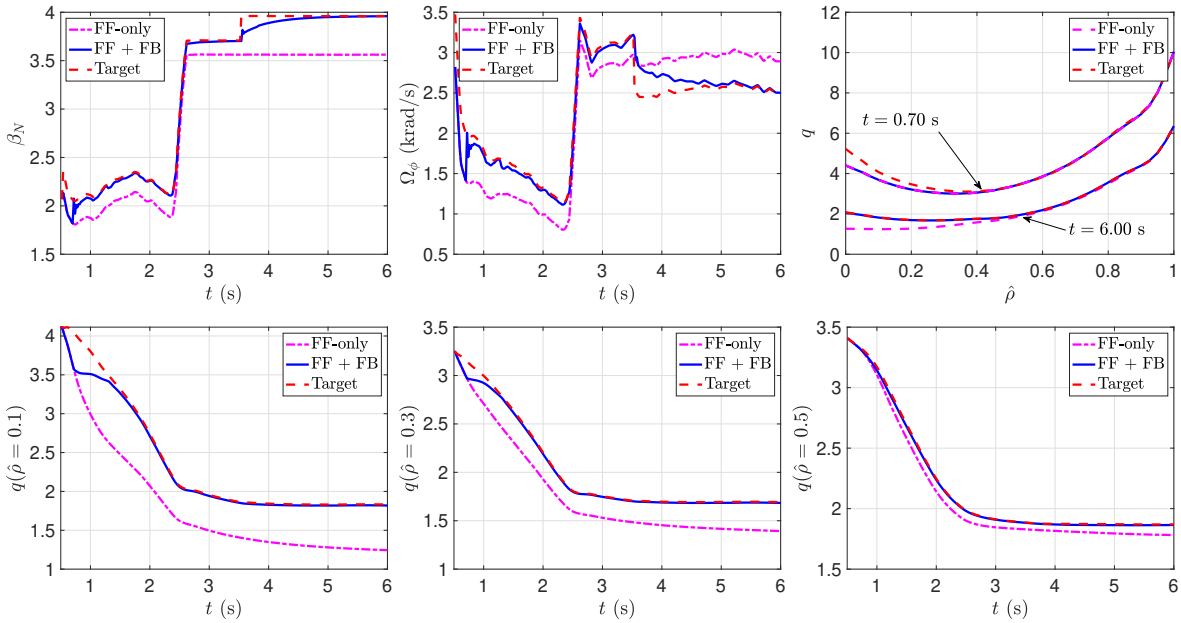

Figure 3: *Plasma-state evolution in FF-only and FF + FB simulations using COTSIM: β_N, Ω_ϕ, and q.*

Fig. 3 shows the time evolutions of β_N, Ω_ϕ, and q during the FF-only and FF + FB simulations, together with the targets $\bar{\beta}_N$, $\bar{\Omega}_\phi$, and $\bar{q}$. With FF-only, it can be seen that all variables are substantially far from their respective targets. Consistently lower q and β_N evolutions are found during the FF-only simulation, and lower ($t \leq 3.5$ s) but then higher ($t > 3.5$ s) values of Ω_ϕ. In the FF + FB simulation, successful β_N, Ω_ϕ, and q regulation are achieved when $t \geq 0.7$ s,

despite employing quite challenging $\bar{\beta}_N$ and $\bar{\Omega}_\phi$ (specially the steps at $t = 2.5$ s and $t = 3.5$ s). In addition, the initial q profiles ($t = 0.7$ s) in FF-only and FF + FB simulations are identical, but convergence toward $\bar{q}$ (e.g. when $t = 6$ s) at $\hat{\rho} \leq 0.5$ is only achieved in the FF + FB case.

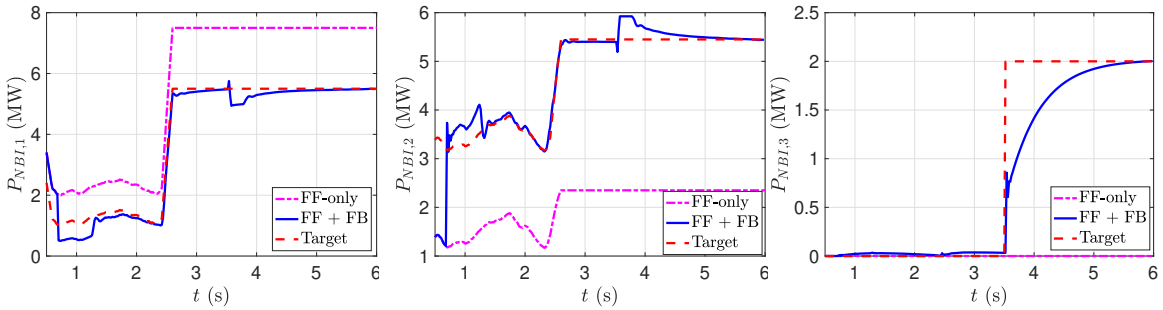

Figure 4: *Inputs during FF-only and FF + FB simulations using COTSIM:* $P_{NBI,1}$, $P_{NBI,2}$, *and* $P_{NBI,3}$.

Fig. 4 shows the time evolutions of $P_{NBI,i}$ ($i = 1,2,3$) during FF-only and FF + FB simulations, together with the target evolutions. The FF-only evolutions are significantly far from the target and FF + FB evolutions, demonstrating the nonlinear capabilities of the control scheme. Also, under FF + FB, $P_{NBI,i}$ are modulated and converge toward the actuator trajectories used to generate the targets, despite the fact that the FB controllers have no such information.

Conclusion and Future Work

The control scheme with a receding-horizon AM optimization has good performance in nonlinear, 1D simulations using COTSIM©. A case with $\Omega_\phi + \beta_N + q$ control by means of NBI has been studied. However, the AM approach is general and can be used with general control objectives. A key advantage of the scheme is that the controllers can be synthesized independently, but are functionally integrated by means of the AM algorithm. Future work may consider the integration of other controllers and actuators with the AM, and experimental testing in DIII-D.

Acknowledgment

This work is supported by the U.S. Department of Energy, Office of Science, Office of Fusion Energy Sciences, Award DE-SC0010661.

References

[1] C. J. Rapson, et al., Experiments on actuator management and integrated control at ASDEX Upgrade, *Fusion Engineering and Design* **123**, (2017) 603–606

[2] E. Maljaars, et al., Actuator allocation for integrated control in tokamaks: architectural design and a mixed-integer programming algorithm, *Fusion Engineering and Design* **122**, (2017) 94–112

[3] M. Kong, et al., Control of neoclassical tearing modes and integrated multi-actuator plasma control on TCV, *Nuclear Fusion* **59**, (2019) 076035

[4] N. M. T. Vu, et al., Tokamak-agnostic actuator management for multi-task integrated control with application to TCV and ITER, *Fusion Engineering and Design* **147**, (2019) 111260

[5] D. A. Humphreys, et al., Novel aspects of plasma control in ITER, *Physics of Plasmas* **22**, (2015) 021806

[6] A. Pajares and E. Schuster, Current profile and normalized beta control via feedback linearization and Lyapunov techniques, *Nuclear Fusion* **61**, (2021) 036006